Available online at www.sciencedirect.com
SCIENCE DIRECT®
Materials and Design 25 (2004) 317–329
Materials & Design
www.elsevier.com/locate/matdes

An investigation of microstructure/property relationships in dissimilar welds between martensitic and austenitic stainless steels

Ramazan Kaçar *, Orhan Baylan

Zonguldak Karaelmas Üniversitesi, Karabük Teknik Eğitim Fakültesi, Metal-Welding Division, Karabük 78100, Turkey

Received 21 May 2003; accepted 15 October 2003

Abstract

The metallurgical characteristics, tensile, hardness, toughness and corrosion resistance of dissimilar welds between X5CrNi18-10 grade austenitic and X20CrMo13 grade martensitic stainless steel have been evaluated. Both austenitic and duplex stainless steel electrodes were used to join this combination, using multipass manual metal arc welding process. Defect free welds were made with each welding consumable. It was found that the tensile strength of weldment, which was produced by duplex electrode (E2209-17), was slightly lower than that of austenitic electrode (E308L-16). The toughness of the both E2209-17 and E308L-16 deposits was acceptable even at low temperature regardless of heat input. Hardness was increased in both welds made with E2209-17 duplex and E308L-16 austenitic electrode along the X20CrMo13/weld metal fusion boundary due to heat annealing and then following high cooling rate. The pitting corrosion resistance of the weld metal made with E308L-16 and E2209-17 filler metal was found acceptable. Although, heat affected zone in the weldment and X20CrMo13 base metal were affected by electrolytic corrosion. This investigation has shown that both filler metals can be used to join austenitic stainless steel to the martensitic stainless steel.

Keywords: Ferritic and martensitic stainless steel; Weldability; Tensile strength; Toughness; Corrosion resistance

1. Introduction

Because of their acceptable corrosion resistance, good mechanical properties and becoming economic, martensitic stainless steel has become increasingly attractive to a number of industry sectors. Austenitic stainless steel has been widely preferred by industry due to its good mechanical properties, outstanding corrosion resistance in a wide range of environment and good weldability. Each type of those grades of stainless steel is welded similarly by using fusion welding technique with or without requirement of special technique. However, there is limited information about microstructure/property relationships in dissimilar welds between austenitic and martensitic stainless steel by using duplex and austenitic stainless steel electrode. Increasing application of these steels will require a better understanding of the issues associated with welds to dissimilar metals. The joining of dissimilar materials is generally more challenging than that of similar materials because of differences in the physical, chemical and mechanical properties of the base metals welded. These differences may also complicate the selection of filler metals compatible to both base metals [1]. Therefore, filler metal selection is often compromised between the two dissimilar metals. There are few constitution diagrams such as Schaeffler [2], Delong [3] and WRC [4], for similar and dissimilar metal joining and predicting the microstructure. However, most of the diagrams currently available do not represent the constitution regime for ferritic and martensitic stainless steel which has the ferrite plus martensite region. Since the WRC-1992 [4] diagram is recommended for ferrite prediction, it is rather awkward to still rely on the Schaeffler diagram for martensite prediction; Schaeffler diagram does not accurately predict microstructure. Therefore, a study was carried out by Kotecki [5] who has investigated the effect of the higher manganese content of the weld filler metal on the constitution regime on diagram. To do this, by plotting the Cr- and Ni-equivalents for the materials on

* Corresponding author. Tel.: +90-370-433-8200; fax: +90-370-4338204.
E-mail address: n_kacar@hotmail.com (R. Kaçar).

0261-3069/$ - see front matter © 2003 Elsevier Ltd. All rights reserved.
doi:10.1016/j.matdes.2003.10.010

the diagram and connecting the base metals by a tie line, the microstructure can be estimated by connecting a point along that tie line (selected as the midpoint) to a tie line to the filler metal composition. The weld metal constitution then lies along the line between the filler metal and base metal midpoint as dictated by the level of dilution.

The dissimilar materials selected for the overall study included an X20CrMo13 grade martensitic stainless steel and X5CrNi18-10 grade austenitic stainless steel. Both austenitic and duplex stainless steel manual metal arc welding electrodes were used to join this combination using multipass manual metal arc welding process. Thus, microstructure/property relationships between austenitic and martensitic stainless steel dissimilar welds were determined in this study. To do this, relationship between hardness, pitting corrosion resistance and % ferrite content related with the weld layer in all weld metal and weldment was investigated. The relationships between microstructure and mechanical properties were also evaluated in detail.

2. Experimental procedure

2.1. Materials and welding procedure

Welding assembly was prepared for dissimilar welds between austenitic stainless steel (X5CrNi18-10) to martensitic stainless steel (X20CrMo13). Both E2209-17 duplex and E308L-16 austenitic welding consumable were selected to join these metals. The chemical composition for the base and consumable was listed in Table 1.

The base materials were supplied in the form of 10-mm plate. These plates were cut into 50×150 mm coupons with a 35° level of each plate to provide 70° groove angle for a single-V-groove butt joint configuration. The root face was 1 mm with root opening of 2.5 mm. All welding was performed using the manual metal arc welding process with 3.2-mm diameter welding electrode. E2209-17 and E308L-16 welding consumable were used in the multipass welds to join X20CrMo13 grade martensitic stainless steel to X10CrNi18-10 grade austenitic stainless steel. The welding parameters were used by the suggestion of welding consumable producer. Due to different thermal conductivity between austenitic and martensitic stainless steel, test samples were preheat treated at 200 °C. Test samples were joined initially in the root and then second followed cover pass by, respectively.

2.2. Mechanical properties

Tensile strength specimens were prepared from weldment. Samples were prepared in the L–T orientation as TS 138. Test was performed using Instron tensile test machine. Scanning electron microscope was utilized to examine the fracture surface of the test sample.

Charpy V-notch (CVN) specimens were also machined from the welded coupons. Samples were prepared in the L–T orientation as TS 269. The L–T orientation represents a sample transverse to the welding direction with the notch located such that testing occurs through the thickness of the weld from root to the cover passes. All notches were located at the centre of the weld deposit. The test was performed at temperature from −50, 0 and 25 °C in order to define the toughness of weld metal. Scanning electron microscopy was also utilized to examine the fracture surfaces of the CVN samples.

Moreover, heat affected zone and weld metal hardness of weldment was measured by future Tech model Vickers micro hardness test machine. Measurement was carried out through the weldment profile in Fig. 1. A 100 g load was used in the test machine.

2.3. Pitting corrosion resistance

Pitting corrosion test was performed at 50 °C as described in ASTM G-48. Two types of samples were tested. The first type consisted of an entire weldment, including both base materials and the fusion zone. The

Table 1
Chemical composition of base and weld metal

	C	Mn	Si	S	P	Cr	Mo	Ni	V	Al	Ti	Cu	N
Chemical composition base metal and welding consumable (wt%)													
X5CrNi18-10	0.040	1.340	0.571	0.035	0.030	17.066	0.516	7.6	0.063	0.010	0.007	0.586	
X20CrMo13	0.220	0.360	0.480	0.001	0.018	12.257	0.037	0.227	0.040	0.083	0.007	0.116	
E308L-16	0.03	0.8	0.8	–	–	19.8	–	10.2	–	–	–	–	
E2209-17	0.03	0.8	0.9	–	–	22.5	3.2	9	–	–	–	–	0.15

	Cr equivalent	Ni equivalent	Cr/Ni equivalent	PRE
X5CrNi18-10	18.43	9.47	1.94	–
X20CrMo13	13.014	7.007	1.85	–
E308L-16	21	11.5	1.82	–
E2209-17	27.05	10.3	2.62	35.46

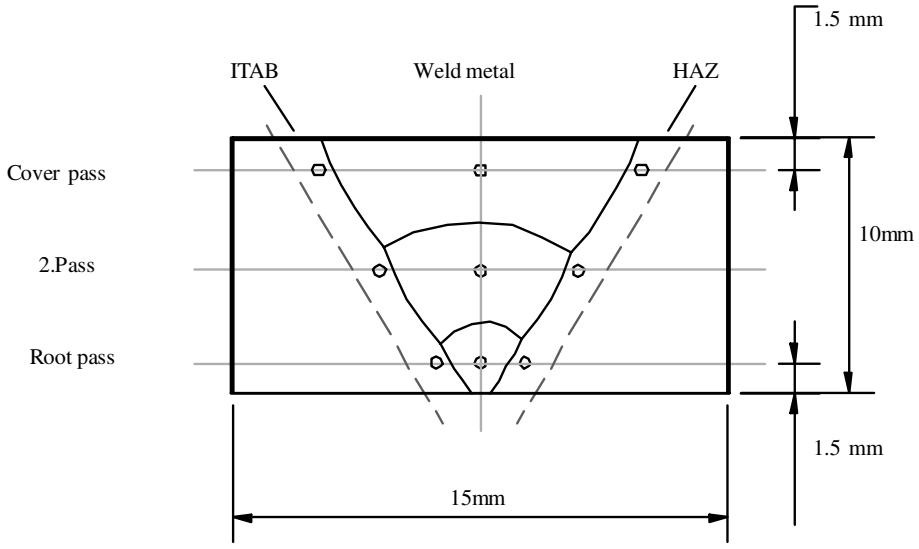

Fig. 1. Hardness determination profile on the weldment.

second type was an all weld metal sample machined out of the fusion zone through the thickness. Since the thickness of the material was 10 mm, standard specimen could not be used and samples of 10×33 mm were used. The specimen was ground through the 600 grit SiC and weighted prior to immersion in solution. The pitting corrosion solution was 6% $FeCl_3 6H_2O$. Samples were immersed in this solution for 72 h and removed and observed every 12 h to note any changes. Following 72 h test period, the samples were carefully scrubbed under running water and then ultrasonically cleaned in methanol for approximately 30 min. Evaluation of pitting was determined by optical microscopy. The pits were counted at magnifications of 50X and measured at 500X. Pits density was determined by dividing the number of pits per unit area.

2.4. Metallurgical characterization and prediction of weld microstructure

Weld cross sections were removed from each combination and grounded through 200–1200 mesh using grinding paper and then polished through 1 μm diamond paste. The samples were electronically etched in 10% oxalic acid at 5 V for 45 s. In the present work, optical examination of samples was carried out using a Nikon DIC microscope. A Camscan Series 4 scanning electron microscope (SEM) with a link energy dispersive X-ray (EDX) analytical system was also used for qualitative weld metal analyses.

Weld metal microstructure constitution regime and % ferrite content can be predicted using Scheaffler diagram for both weldments. Due to high alloy elements in the weld metal that was made with E2209-17 weld consumable, ferrite number (FN) must be calculated using the WRC-1992 diagram [4]. However, this diagram did not take martensite formation therefore Kotecki was rearranged to the diagram which is enabling to show martensite boundary [5]. Therefore, prediction of weld microstructure was carried out using this diagram (Fig. 2).

Ferrite number measurements were also carried out using ferritscope (type Fe8e3). All measurements were obtained on longitudinal sections in the weld metal and heat affected zone rather than transverse section in order to better quantify variation within given pass. Three measurements were taken at three different locations within each pass. The results were then averaged to obtain ferrite number of each pass. The % ferrite content was calculated by dividing the ferrite number with 1.4.

3. Results

The dissimilar X5CrNi18-10/X20CrMo13 metal combination was welded with duplex E2209-17 and austenitic E308L-16 filler metal. Fig. 3(a) and (b) shows microstructure profile of the X5CrNi18-10/E2209-17/X20CrMo13 and X5CrNi18-10/E308L-16/X20CrMo13 weldment, respectively. The microstructure of this combination consists of austenite matrix (white) with both skeletal and acicular ferrite (dark etching).

The relationship between all weld pass and % ferrite content in the weldment was determined and result is shown in Fig. 4.

Ferrite measurement indicates that 59 FN (42% ferrite content) and 17 FN (12% ferrite content) in the weld metal, which was obtained using E2209-17 and E308L-16 filler metal, respectively, was measured in the root pass of the weldment. Based on this modified WRC-2000 diagram, 20 FN (14% ferrite content) was calculated in the root pass of E308L-16 weld metal while

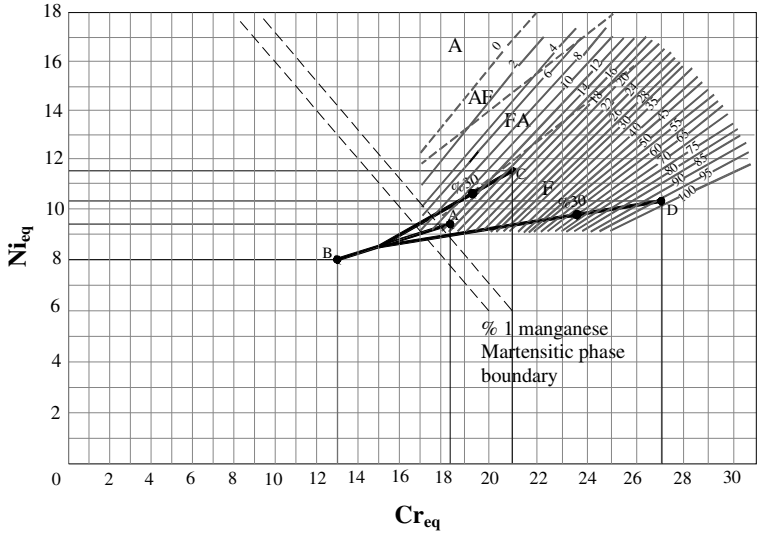

Fig. 2. Welding Research Council diagram for duplex stainless steel weld metal.

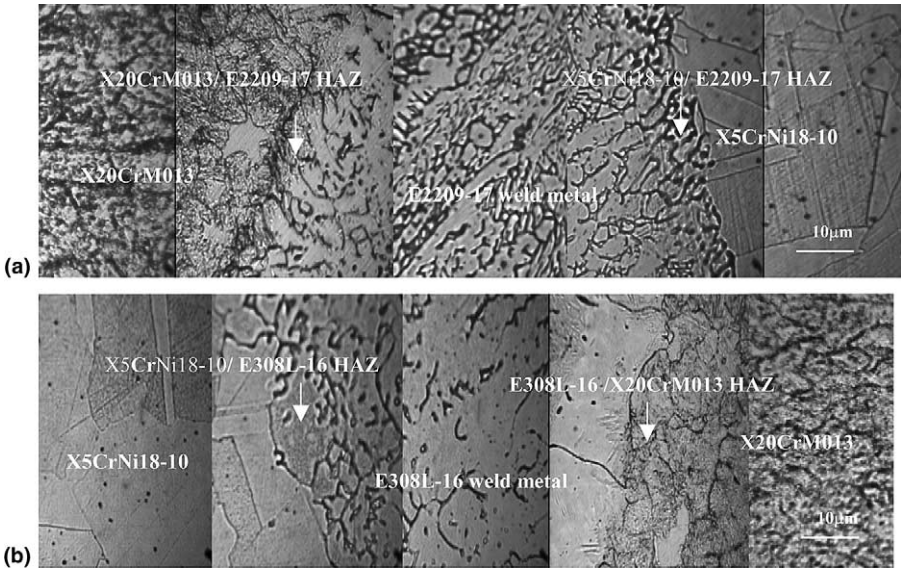

Fig. 3. (a) Microstructure of the X5CrNi18-10/E2209-17/X20CrMo13 weldment. (b) X5CrNi18-10/E308L-16/X20CrMo13 weldment (X50).

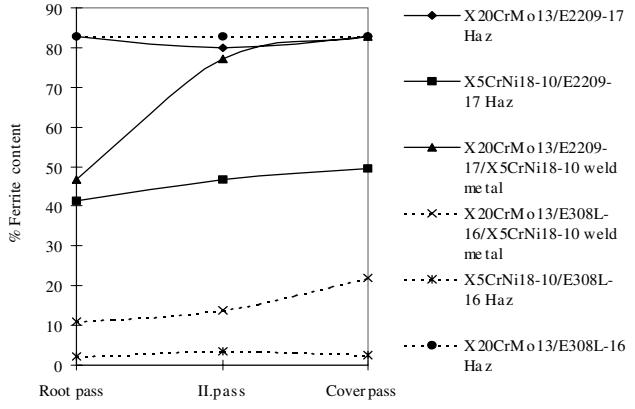

Fig. 4. The relationship between all weld pass and % ferrite content in the weldment.

it was determined as a 95 FN (68% ferrite content) in a root pass of the E2209-17 weld metal. Results clearly show that WRC-2000 diagram ferrite estimation and result got from ferritscope measurement are similar and consisted with each other in the root pass of the E308L-16 weld metal. However, by application of high alloyed filler metal such as E2209-17, WRC diagram slightly overestimated the FN as compared with the ferritscope measurement. It also clarifies that dilution in the root pass of the E2209-17 weld metal is 35%.

In the second pass of the E2209-17 and E308L-16 weld metal, % ferrite content was measured 109 FN (78) and 20 FN (14), respectively. Result shows that ferrite content of the E2209-17 weld metal was increased higher than E308L-16 weld metal with regard to chemical

composition of filler metal, dilution from base metal and cooling rate.

The ferrite content of the cover pass was measured 120 FN (85) in E2209-17 weld metal, meanwhile, it was determined 22FN (15) in E308L-16 weld metal. Result shows that there is an increase in ferrite content of the weld metal from root through cover pass. It was noticed that increase in the ferrite content of E2209-17 weld metal is much higher than that of E308L-16 weld metal. It may be explained that high cooling rate on the cover pass of the weld causes significant amount of ferrite due to duplex structure of filler metal and high cooling rate of weldment but increase on the E308L-16 weld metal comes from dilution from martensitic base metal and cooling rate.

In addition, relationship between ferrite content and weld layer in the X20CrMo13/E2209-17 and X20CrMo13/E308L-16 heat affected zone was evaluated. It was found that the ferrite content of both the heat affected zones was measured approximately 120 FN (85) in all pass. Result indicates that during the heat affected zone ferrite measurement; probe of the ferritscope was affected from martensitic stainless steel base metal that has 100% magnetic phase.

Furthermore, the relationship between ferrite content and weld layer in the X5CrNi18-10/E2209-17 and X5CrNi18-10/E308L-16 heat affected zone was also evaluated. It was found that in all pass of the X5CrNi18-10/E308L-16 heat affected zone ferrite content was measured approximately 4.5 FN (3). Result shows that ferrite content of the austenitic filler metal is found at low level as expected due to its chemical composition. Austenitic base metal may also effect to the ferritscope measurement in all pass of X5CrNi18-10/E308L-16 heat affected zone. However, X5CrNi18-10/E2209-17 heat affected zone ferrite content was measured approximately 56 FN (40), 67 FN (48) and 73 FN (52) in root, second and cover passing, respectively. This small increase on the ferrite content can be explained less dilution from austenitic base metal from root the cover pass resulting tend got more ferrite phase in duplex structure. The high cooling rate may also accelerate to the ferrite formation in this region.

It was notified that columnar grain in the weld metal was growing up isotrophically to the direction of the base metal that has higher thermal coefficient. Moreover, in some grain chromium depletion was also observed in both X20CrMo13/E308L-16 and X20CrMo13/E2209-17 weld metal fusion boundary due to high carbon content of the martensitic stainless steel.

3.1. Mechanical properties

3.1.1. Tensile strength

Table 2 shows mechanical property data, which include tensile, yield strength and elongation values for dissimilar joints between martensitic and austenitic stainless steel.

Results show that X5CrNi18-10/E2209-17/X20CrMo13 combination was exhibited lower tensile, yield strength as well as elongation when it was compared with weldment that was obtained by E308L-16 filler metal. However, the joint strength was found acceptable because all test sample was broken from X20CrMo13 base metal. The fracture surface of the tensile test sample was evaluated and general EDS analysis was carried out. The representative micrograph of the fracture surface and EDS analysis result is given in Fig. 5(a) and (b).

Tensile test sample fracture surface clearly showed that ductile fracture occurred in both weldments. As can be seen in Table 2, high level of elongation obtained on the both weldments was also support to the ductile fracture. Meanwhile, EDS result verified that fracture occurred on the martensitic stainless steel base metal.

3.1.2. Weld metal impact toughness

The CVN impact toughness results for the X5CrNi18-10/E2209-17/X20CrMo13 and X5CrNi18-10/E2209-17/X20CrMo13 weld combinations are given in Fig. 6.

The lower impact energy was roughly 70 J at the temperature −50 °C that was obtained from test sample which was produced by E2209-17 duplex electrode. When the test temperature is reached to 0 °C, the impact energy was found 84 J. Approximately 115 J impact energy was obtained while test temperature exhibited 25 °C. However, second lower impact energy (84 J) was found from test sample which was produced by E308L-16 austenitic electrode. When the test temperature is reached to 0 °C the impact energy was found 104 J. Approximately 110 J impact energy was obtained at the test temperature of 25 °C.

The fracture surface of the weldment that was obtained by E2209-17 and E308L-16 filler metals was also evaluated in SEM and the result is shown in Fig. 7(a) and (b), respectively. The test sample which was tested at −50 °C exhibited a mixed cleavage-type showing relatively flat surface and ductile fracture. However, at 0 °C all test sample exhibited entirely ductile fracture but some local cleavage-type fracture showing relatively flat surface was also observed in the X5CrNi18-10/E2209-17/X20CrMo13 weldment (Fig. 7(c) and (d)).

Table 2
Mechanical properties of weldment

Property	X5CrNi18-10/E308L-16/X20CrMo13 combination	X5CrNi18-10/E2209-17/X20CrMo13 combination
Tensile strength	800 (MPa)	880 (MPa)
Yield strength	512 (MPa)	618 (MPa)
Elongation (%)	36	46

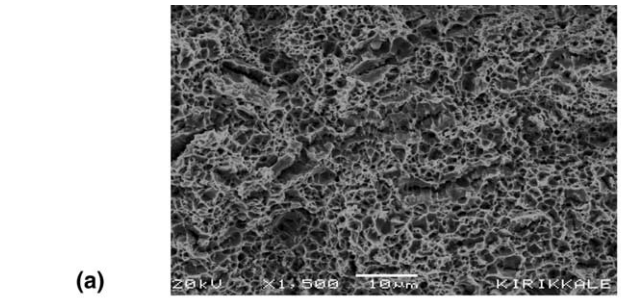

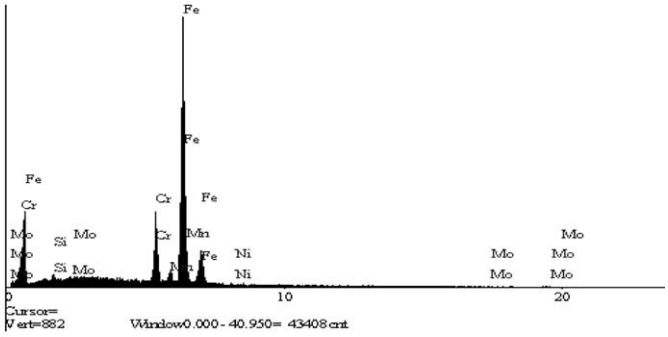

(b)

Elt.	Line	Intensity (c/s)	Conc		
Si	Ka	5.93	0.654	wt.%	
Cr	Ka	107.20	11.819	wt.%	
Mn	Ka	0.76	0.096	wt.%	
Fe	Ka	455.42	86.742	wt.%	
Ni	Ka	0.91	0.262	wt.%	
Mo	La	1.67	0.426	wt.%	
			100.000	wt.%	Total

Fig. 5. (a, b) Tensile test sample fracture surface and EDS analysis results.

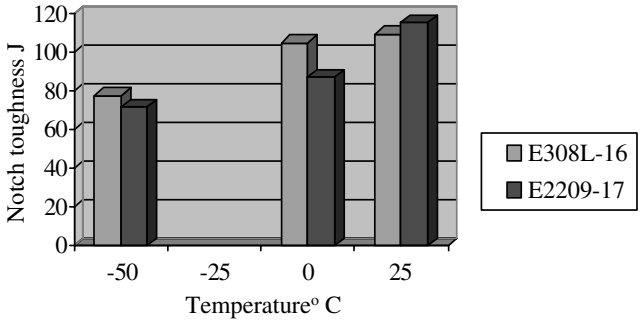

Fig. 6. Charpy impact energies of weldment.

As can be seen Fig. 7(e) and (f), test temperature was set up to 25 °C, fracture surface of the both weldments is exhibited ductile fracture. In the dimple of the crystal some second phase particle was also observed in both weldments.

3.1.3. Hardness results

The weld metal and heat affected zone hardness of the weldment was determined so, the relationship between % ferrite content and hardness related with the weld pass was investigated. Result is given in Fig. 8.

The maximum hardness of weld metal that was produced by E308L-16 filler metal was measured approximately 290 Vh in the root pass, while % ferrite content was obtained 12. While the hardness was decreased to the 230 Vh in the second pass of weld metal, in the cover pass it reached up to 270 Vh. However, % ferrite content in the weld metal was increased from 14 to 16. There seems to be a controversy between decreasing hardness and raising % ferrite content from the root to the cover pass of the weld metal.

In addition, the relationship between % ferrite content and E308L-16/X20CrMo13 heat affected zone hardness was determined. Maximum hardness in the E308L-16/X20CrMo13 heat affected zone was measured approximately 330 Vh in the root pass. Hardness was decreased to 290 Vh in the second pass of HAZ. It was measured approximately 300 Vh in the cover pass. The result indicates that maximum hardness was obtained in the root pass of the heat affected zone due to low heat input resulting in higher cooling rate. The second pass hardness was found lower than root as well as cover passes due to heat treatment effect of cover pass. However, heat affected zone ferrite content was found 85 Vh in all weld passes. There seems to be no relationship between hardness and % ferrite content in the HAZ.

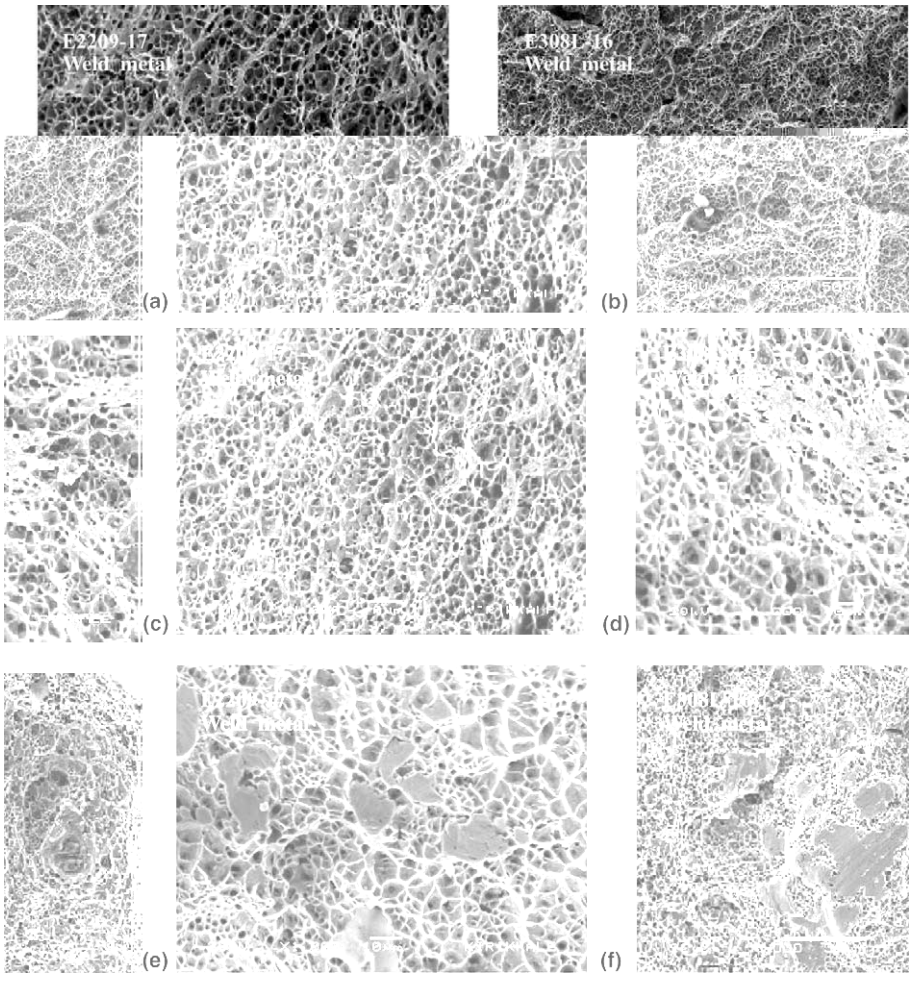

Fig. 7. (a–f) Fracture surface of the charpy impact test sample.

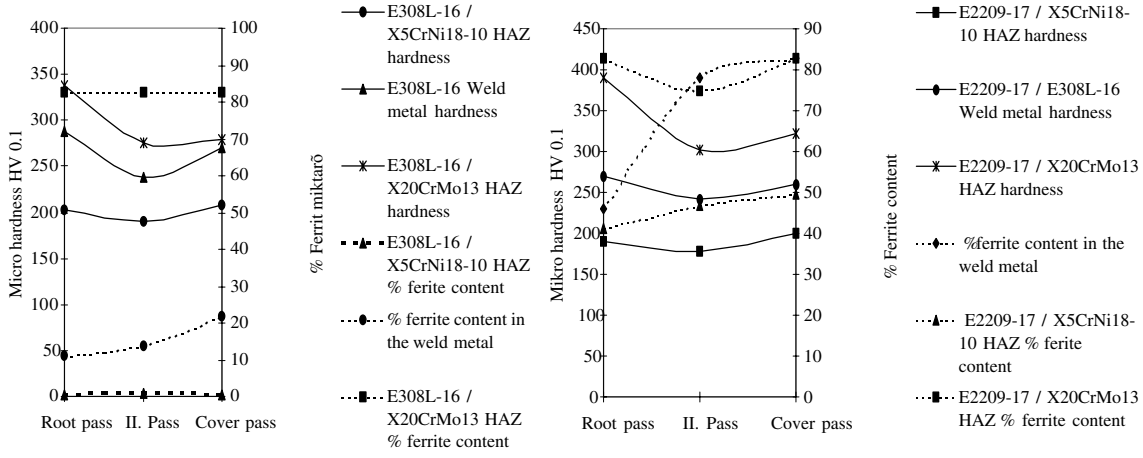

Fig. 8. Relationship between hardness and % ferrite content related to the weld pass in the weldment.

Meanwhile, hardness in the E308L-16/X5CrNi18-10 heat affected zone was measured approximately 200 Vh in the root and cover pass, while it was decreased to the 192 Vh in the second pass. Softer regions along this boundary were found in the second pass of the weld. However, the heat affected zone % ferrite content was found approximately 3 in all weld passes. There seems to be no relationship between hardness and % ferrite

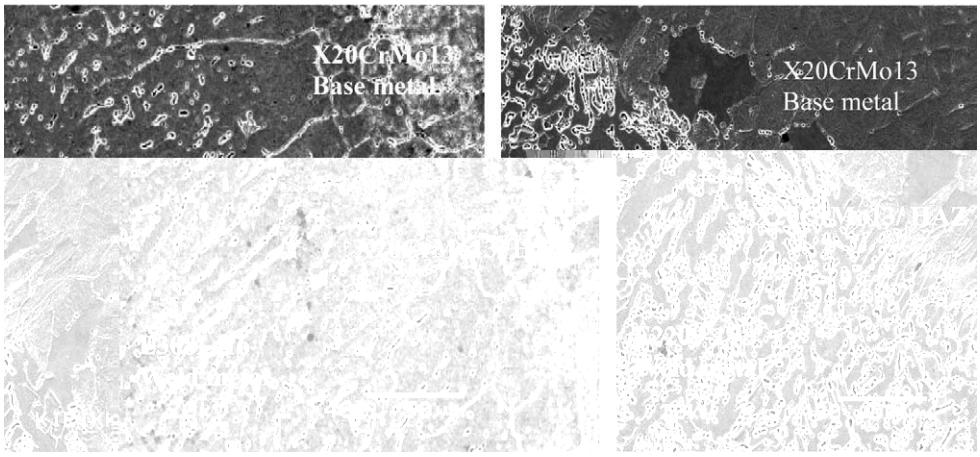

Fig. 9. (a, b) Micrograph of X20CrMo13/HAZ structure.

content in the HAZ. The effect of nonmagnetic austenitic phase on the ferrite measurement of the HAZ has to be considered.

Furthermore, maximum hardness of weld metal that was produced by E2209-17 filler metal was measured averaged 270 Vh in the root pass, while % ferrite content was obtained approximately 48. The hardness was decreased to the 248 Vh in the second pass of weld metal, while % ferrite content measured 78. Hardness reached up to 260 Vh, meanwhile % ferrite content determined 85 in the cover pass of weld metal. The result indicates that the hardness of the weld metal was decreased in contrast to increase in the % ferrite content of the second pass of weld metal. This could be attributable to the heat treatment effect of cover pass on the second pass weld bead.

When the relationship of % ferrite content between the E2209-17/X20CrMo13 heat affected zone hardness was investigated, it was found that higher level of hardness is exhibited in the root pass of the E2209-17/X20CrMo13. It was measured approximately 398 Vh, while % ferrite content was obtained averaged 85. However, hardness was decreased to approximately 305 Vh in the second pass, it was slightly increased on the cover pass where it was measured approximately 320 Vh. The heat affected zone ferrite content was found approximately 83 in second pass while it measured 85 in the cover pass. There seems to be no relationship between hardness and % ferrite content in the HAZ. Result noticed that hardness of the E2209-17/XCr20Mo13 heat affected zone was decreased from root to the cover pass regardless of increasing ferrite content. This could be explained that along the heat affected zone martensitic structure can occur due to higher level dilution from martensitic stainless steel base metal which had 0.22 (wt%) carbon in the chemical composition. Due to low heat input in the root pass might also affect the hardness resulting of high cooling rate of the weldment.

In addition, hardness in the E2209-17/X5CrNi18-10 fusion boundary was measured approximately 195 Vh in the root and cover pass, while it was decreased to approximately 190 Vh in the second pass. Softer regions along this boundary were found in the second pass of the weld. However, heat affected zone % ferrite content was found approximately 42, 48 and 52 in root, second and cover pass, respectively. There seems to be no relationship between hardness and % ferrite content in the HAZ. Due to high level dilution from austenitic base metal, hardness and % ferrite content was determined similar in the HAZ.

A representative microstructure along the E308L-16 and E2209-17/X20CrMo13 heat affected zone is shown in Fig. 9(a) and (b), respectively. This micrograph clearly shows that carbide precipitation decorates these boundaries resulting from carbon migration out of the martensitic stainless steel. Those of carbide may become also responsible HAZ hardness.

3.2. Pitting corrosion test

The corrosion test of the weld metal was conducted in two ways. Initial testing was carried out on both entire weldment by immersing the entire joint cross section including the base materials into corrosive solution at 50 °C for 72 h. The second pitting corrosion test was conducted on both all weld metal samples machined from the weldment. The pitting corrosion results were tabulated as pit density on the weld layer related with % ferrite content. In the both weldment samples, the X20CrMo13 type martensitic stainless steel and HAZ were preferentially attached by the solution, resulting in complete dissolution of the martensitic base metal. The weight loss from the weldment and all weld metal was determined.

The greater weight loss (0.817 g) was obtained in the X20CrMo13/E2209-17/X5CrNi10-18 combination ra-

ther than X20CrMo13/E308L-16/X5CrNi10-18 combination (0.715 g). However, weight loss in X20CrMo13/E2209-17/X5CrNi10-18 and X20CrMo13/E308L-16/X5CrNi10-18 all weld metal was found to be 0.278 and 0.257 g, respectively. Result clearly showed that weight loss was higher in the X20CrMo13/E2209-17/X5CrNi10-18 weld metal. Average pit density also supports this result (Fig. 10).

Relationship between pit density and % ferrite content related with weld layer in the both weldments was also determined. Results are given in Fig. 10. In the weldment sample, the martensitic stainless steel base metal and heat affected zone was preferentially attacked by the solution, resulting in incomplete dissolution of the martensitic stainless steel base metal and HAZ. Therefore, the pitting density measurement was carried out from root to cover pass in the weld metal and X5CrNi 10-18/weld metal heat affected zone of the weldment that was obtained by E2209-17 and E308L-16

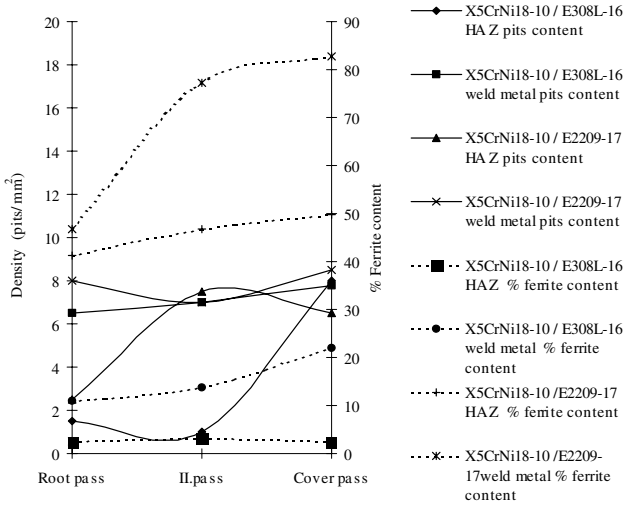

Fig. 10. Relationship between pit density and % ferrite content related with the weld layer on the both weldments and all weld metal.

filler metals. The correlation between pit density result and % ferrite content in the all weld layer was investigated. It was found that the pit density was obtained 8 pits/mm^2 in the root pass of the E2209-17 weld metal, while ferrite content was measured 42%. In the second pass of the weld metal, averaged pit density was measured 7 pits/mm^2 while 78% ferrite content was determined. However, pit density and ferrite content was reached up to 8 pits/mm^2 and 85% in the cover pass of the weld metal. In addition, the pit density was obtained averaged 6.2 pits/mm^2 in the root pass of the E308L-16 weld metal, while ferrite content was measured 12%. In the second pass of the weld metal, averaged pit density was measured 7 pits/mm^2 while 14% ferrite content was determined. However, pit density and ferrite content was reached up to 8 pits/mm^2 and 15% in the cover pass of the weld metal.

The correlation between pit density result and % ferrite content in the all weld layer of X5CrNi18-10/E2209-17 heat affected zone was investigated. It was found that the pit density was obtained averaged 2.2 pits/mm^2 in the root pass, while ferrite content was measured 40%. In the second pass of the weld layer, averaged pit density was measured approximately 7.5 pits/mm^2 while 48% ferrite content was determined. However, pit density and ferrite content was decreased to 6 pits/mm^2 and 52% in the cover pass of the weld layer. In addition, the pit density was obtained averaged 1.5 pits/mm^2 in the root pass of the X5CrNi18-10/E308L-16 heat affected zone, while ferrite content was measured 3%. In the second pass of the weld layer, averaged pit density was measured 1.2 pits/mm^2 while 4.5% ferrite content was determined. However, pit density and ferrite content was reached up to 7 pits/mm^2 and 3%, respectively, in the cover pass of the weld layer.

Relationship between pit density and % ferrite content related with weld layer in the all weld metal was also determined. Results are given in Fig. 11.

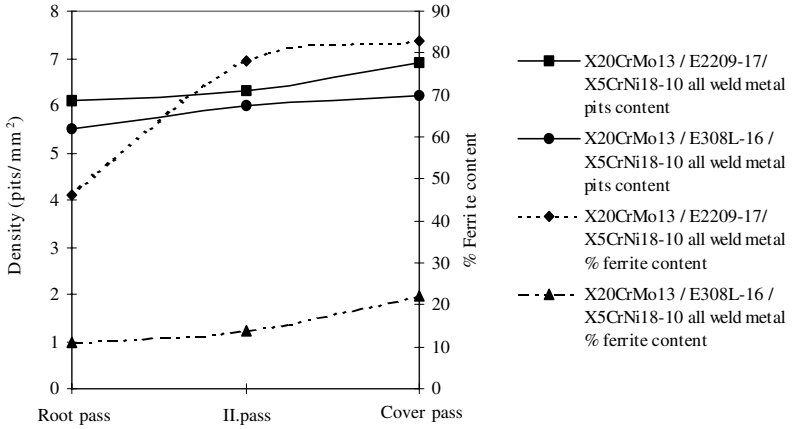

Fig. 11. The relationship between pit density and % ferrite content related to the weld pass in the X20CrMo13/E308L-16/X5CrNi18-10 and X20CrMo13/E2209-17/X5CrNi18-10 all weld metal.

The correlation between pit density result and % ferrite content in the all weld layer was found that the pit density was obtained 6 pits/mm^2 in the root pass of the E2209-17 weld metal, while ferrite content was measured 42%. In the second pass of the weld metal, averaged pit density was measured 6.2 pits/mm^2 while 78% ferrite content was determined. However, pit density and ferrite content was reached up to 7 pits/mm^2 and 85%, respectively, in the cover pass of the weld metal. In addition, the pit density was obtained averaged 5.5 pits/mm^2 in the root pass of the E308L-16 weld metal, while ferrite content was measured 12%. In the second pass of the weld metal, averaged pit density was measured 5.8 pits/mm^2 while 15% ferrite content was determined. However, pit density and ferrite content was reached up to 6 pits/mm^2 and 22% in the cover pass of the weld metal.

4. Discussion

The results of this investigation have shown that austenitic stainless steel can be welded to martensitic stainless steel using either duplex E2209-17 or austenitic filler material E308L-16. Both combinations exhibited good weldability and free from fabrication related defects such as solidification cracking, liquidation cracking, porosity and incomplete fusion. In general, from a procedural point of view there is a need preheat treatment before the welding the dissimilar combinations using either welding consumable.

4.1. Microstructure evolution

Fig. 3(a) and (b) the shows clearly microstructure profile of X5CrNi18-10/E2209-17/X20CrMo13 and X5CrNi18-10/E308L-16/X20CrMo13 weldment, respectively. A representative microstructure along the E2209-17 and E308L-16/X20CrMo13 heat affected zone is also shown in 9a and b, respectively. This micrograph clearly shows the fusion boundary microstructure of E308L-16/X20CrMo13 dissimilar welds that has type II grain boundaries. Type of grain boundaries was explained by Rowe et al. [6] who referred K. Asami and T. Sakai's studies which indicate that normal epitaxial nucleation during the solidification along the fusion boundary gives rise to grain boundaries that are continuous from the base metal into weld metal across the fusion boundary. These boundaries are perpendicular to the fusion boundary and have been referred to as Type I boundaries. In dissimilar welds, where an austenitic weld metal and ferritic base metal exist, a type II of boundary runs roughly parallel to the fusion boundaries. Nelson et al. [7] also reported that when the base and weld metal exhibit different crystal structures (BCC/FCC) at the solidification temperature, nucleation of the solid weld metal occurs on the heterogeneous sites on the partially melted HAZ grain at the fusion boundary. These boundaries typically have no continuity across the fusion boundary to the grain boundaries in the base metal. This may suggest that the solidification behavior in this partially mixed region adjacent to the fusion boundary may be different from that of the bulk zone or that solid state transformations following solidification may result in the formation of these boundaries [1].

It was not observed in Type II boundaries, especially E2209-17/X20CrMo13 fusion boundary. Barnhouse also referred to Wu and Patched's studies in which was reported that the ferritic solidification of duplex stainless steels eliminates Type II grain boundaries from occurring. Result from Table 2 also indicates that the Cr eq/Ni eq ratio of the duplex stainless steel filler metal is calculated (2.62) which means solidification mode of the weld metal occurred initially in δ-ferrite form. When the base and weld metal exhibit the same crystal structure at the solidus temperature, standard weld metal epitaxial growth may occur despite significant differences in composition [8].

The high hardness along the fusion boundary in HAZ region of both weldments is attributed to the formation of acicular martensitic structure, which results in significantly greater hardness along the E2209-17 fusion boundary rather than along the E308L-16 fusion boundary. The modified WRC diagram also in Fig. 2 indicates the formation of martensitic boundary in both martensitic HAZ of weldments. Within a short distance from the heat affected zone, hardness in all welds passes rapidly to the level of base metal.

Carbide precipitation decorates these HAZ resulting from carbon migration out of the martensitic stainless steel into the more highly alloyed but lower carbon fusion zone such as E2209-17/X20CrMo13 fusion boundary (Fig. 9(a)).

In addition, the columnar grain orientation to the direction of martensitic base metal was observed in both weldments due to heat transformation coefficient of the martensitic stainless steel base metal higher than that of austenitic base metal. The microstructure of weld metals consist with both skeletal, Widmanstaetten and acicular ferrite which depend the solidification mode, chemical composition and cooling rate [9]. The microstructure of the weldmetal in Fig. 3 supports the Kotecki's modified WRC diagram which enables the ferritic and martensitic phase boundary.

4.2. Toughness behavior and tensile strength of weldment

The charpy impact test results for both combinations are summarized in Fig. 6. Both combination exhibited good impact toughness over a wide range of temperature. Due to microstructure, duplex and austenitic stainless steel does not exhibit upper/lower shelf tran-

stition such as ferritic weld metal. Therefore, charpy impact test of the weld metal at both combinations was carried out at a temperature of −50, 0 and 25 °C. Result indicates that the impact thoughness exhibited gradual decrease with temperature. It is interesting to note that the toughness of duplex E2209-17 weld deposits exceeds that of E308L-16 deposits at room temperature. This may be explained by the structure of duplex weld deposit. Because, duplex stainless steel contains approximately 50% ferrite phase, which provides strength, which is embedded by austenite matrix where ductility comes from. Duplex E2209-17 deposits also exhibit comparable toughness at temperatures down to −50 °C.

Examples of the fracture surface appearance of test samples are shown in Fig. 7(a)–(f). As seen in Fig. 7(a) and (b), both weld metals showed predominantly a ductile fracture appearance of microvoid coalescence (MVC) at room temperature. The ductility plus the high toughness of the stainless steel resulted in an impact toughness of the weld metal approximately 115 J (Fig. 6).

The test samples fractured at 0 °C again showed cracking only in the ferritic base steel. Fig. 7(c) and (d) shows ductile fracture behavior in combination of transgranular fracture and MVC surface. The lower notch toughness value of approximately 100 J can be attributed to the change in fracture mode associated with the lower test temperature (Fig. 6). The second phase particle in the dimple was also supported by the ductile fracture behavior.

The fracture surface of test samples broken at −50 °C again showed entirely ductile fracture behavior but due to the low test temperature, some local transgranular fracture by quasi-cleavage was observed (Fig. 7(e) and (f)). This fracture appearance is consistent with the low average impact energy of approximately 80 J (Fig. 6).

Tensile test results indicate that X5CrNi18-10/E2209-17/X20CrMo13 combination exhibited lower tensile, yield strength as well as elongation when it was compared with weldment that was obtained by E308L-16 filler metal. Although, all test sample was broken from X20CrMo13 base metal, it can be attributable to the characteristics of the dissimilar weldment. Because, during the testing when the strength was reached to the yield point, neck initially occurred on X20CrMo13 base metal side of the test sample. By increasing applied load on the another neck started to occur on the austenitic base metal side of X5CrNi18-10. After a while, the load on the test sample reached the maximum strength and all resulting test samples were fractured on the first neck that occurred on martensitic base metal side. None of the test samples were broken either in weld metal and martensitic HAZ of weldment. EDS analysis in Fig. 5(a) and (b) also supported this result. The lower tensile, yield strength as well as elongation of X5CrNi18-10/E2209-17/X20CrMo13 combination rather than X5CrNi18-10/E308L-16/X20CrMo13 combination can be explained by ductility of the austenitic filler metal as well as higher degree of second phase particle in the martensitic base metal. However, the joint strength was found acceptable in both combinations. The representative micrograph of the fracture surface is given in Fig. 5(a) and (b) which supports to the higher degree ductility.

4.3. Hardness measurement

The result from Fig. 8 showed that there is a controversy between hardness raise and % ferrite content in the root pass of the weld metal that was obtained by E308L-16 filler metal. It may be concluded that high level dilution from martensitic stainless steel and low heat input in the root pass exhibited higher level hardness but decrease on the % ferrite content can be explained by austenitic stainless steel filler metal that has normally 3–5% ferrite.

In addition, it seems that there is no relationship between hardness and % ferrite content in the E308L-16/X20CrMo13 heat affected zone (Fig. 8). This may be attributed to heat annealing followed by high cooling rate during the welding process which tends to increase heat affected zone hardness. Meanwhile, decrease in the hardness of second pass in the heat affected zone can be explained by the heat treatment. As known that during the welding of cover pass, heat generated from arc makes tempering effect on the second pass weld bead. Normally, differential on the hardness increasing related with the % ferrite content may be expected but all weld pass % ferrite content was found similar. It is evident that the probe of the ferritscope was affected by martensitic stainless steel due to narrow heat affected zone.

The result from Fig. 8 also showed that there seems to be no relationship between hardness and % ferrite content in the E308L-16/X5CrNi18-10 heat affected zone. It may be concluded that austenitic stainless steel heat affected zone exhibited lower hardness in all weld pass when it is compared with martensitic stainless steel heat affected zone and weld metal due to austenite phase in their microstructure. Slight decrease in the hardness at the second pass fusion boundary can be explained by the heat treatment that comes from tempering effect of cover pass on it. Differential on the hardness increasing related with the % ferrite content may also be expected but all weld pass % ferrite content was found similar. It is evident that the probe of the ferritscope was effected by austenitic stainless steel due to narrow heat affected zone.

Furthermore, there seems to be a controversy between hardness raise and % ferrite content in the second

pass of the E2209-17 weld metal (Fig. 8). Slight decrease in the hardness at the second pass weld metal can be also explained by the heat treatment that makes tempering effect of the second pass weld metal.

In addition, result from Fig. 8 also showed that there is no relationship between hardness and % ferrite content in the E2209-17/X20CrMo13 heat affected zone. Normally, differential on the hardness increasing related to the % ferrite content may be expected but all weld pass in the fusion boundary, % ferrite content was found similar. It is evident that the probe of the ferritscope was affected by martensitic stainless steel due to narrow heat affected zone. High level hardness exhibited in the fusion boundary can be explained by the heat annealing followed by high cooling rate during the welding process that may increase hardness to maximum level in the root and cover pass.

No relationship could be found between hardness and % ferrite content in the E2209-17/X5CrNi18-10 heat affected zone. It may be concluded that austenitic stainless steel heat affected zone is exhibited lower hardness in all weld pass when it is compared with martensitic stainless steel HAZ and weld metal due to austenite phase in their structure. Slight decrease in the hardness at the second pass fusion boundary can be explained by the heat treatment that makes tempering effect of cover pass on it. Differential on the hardness increasing related with the % ferrite content may also be expected but all weld pass % ferrite content was found similar. It is evident that the probe of the ferritscope was affected by austenitic stainless steel due to narrow heat affected zone. High level of % ferrite content in the weldment, when it is compared with combination that was obtained by E308L-16 filler metal, can be explained by increasing ferrite phase due to high cooling rate during the welding process.

4.4. Pitting corrosion test

The corrosion test of the weld metal interestingly showed that pit density was increased with higher ferrite content from root to the cover pass of the E308L-16 weld metal but slightly decreased in the pit density in contrast to higher ferrite content in the second pass of the E2209-17 duplex weld metal. Affected, pitting corrosion resistance of the weld metal increases by austenite. The small decrease in the pit density of second pass of the E2209-17 weld metal may be explained by chemical composition of the weld metal which has more impurity or second phase particle.

The correlation between pit density result and % ferrite content in the all weld layer of X5CrNi18-10/E2209-17 heat affected zone was investigated. It was interestingly noted that pit density was increased with higher ferrite content from root to the cover pass of the X5CrNi18-10/E2209-17 HAZ but small decrease was observed in the pit density in contrast to higher ferrite content of the cover pass. Normally, pitting corrosion resistance of the weld metal increases by austenite. The small decrease in the pit density of cover pass of the E2209-17 weld metal may be explained by chemical composition of the weld metal which has more Cr_2N precipitation. It was also interestingly noted that huge increase was observed in the pit density of the cover pass of the X5CrNi18-10/E308L-16 HAZ in contrast to lower ferrite content. It may be also explained that the dilution in the X5CrNi18-10/E308L-16 HAZ occurs higher than weld metal, therefore austenite amount of this region is much higher than that of other place. This provides significant pitting corrosion resistance to the steels. Higher amount of pit density on the cover pass of the weld metal can be explained by chemical composition and high amount of impurity that comes from filler metal.

The relationship between pit density and % ferrite content related with weld layer in the all weld metal was also determined. It was noticed that pit density was slightly increased with higher ferrite content from root to the cover pass of the E308L-16 and E2209-17 weld metal due to increase in the pitting corrosion resistance of the weld metal by austenite. However, it was noticed that the pitting density of the E308L-16 weld metal was lower than E2209-17 weld metal due to higher austenite content in the matrix.

Consequently, the pitting corrosion resistance of the all weld metal and weldment was obtained with E308L-16 filler metal slightly better than weld made with E2209-17 filler metal due to higher level of austenite and reduced chromium nitride precipitation.

5. Conclusions

On the basis of the research work described in this paper, the following conclusions can be drawn:

1. The results of this investigation have shown that austenitic stainless steel can be welded to martensitic stainless steel using either duplex E2209-17 or austenitic filler material E308L-16. From a procedural point of view, there is a need for preheat treatment before welding the dissimilar combinations using either welding consumable.
2. The tensile strength of weldment, which was produced by duplex electrode (E2209-17), was slightly lower than that of austenitic electrode (E308L-16). However, both dissimilar weldments exhibit an acceptable joint strength.
3. The microhardness was increased in both welds made with E2209-17 duplex and E308L-16 austenitic electrode along the X20CrMo13/weld metal fusion boundary due to heat annealing and then follow high cooling rate.

4. The impact toughness of the both E2209-17 and E308L-16 deposits was acceptable even at low temperature regardless of heat input. The test sample given with all test temperature exhibits ductile fracture behavior due to the high impact toughness of the stainless steel.
5. Although, the pitting corrosion resistance of the all weld metal and weldment which was obtained with E308L-16 filler metal slightly better than weld made with E2209-17 filler metal due to higher level of austenite and reduced chromium nitride precipitation. Consequently, both filler metal pitting corrosion resistance was found acceptable.
6. Microstructure of the weldment supports the Kotecki's modified WRC diagram which enables to exhibit martensitic and ferritic phase boundary.
7. Type II grain boundaries in the E308L-16/XCr20-Mo13 fusion boundaries occurred in contrast to E2209-17/XCr20Mo13 fusion zone.

Acknowledgements

The authors thank Mr. Dr. Selçuk Aktürk of Kırıkkale University, Mech. Eng. Mr. Erkan Koç of Noksel Company, TR for their kind supply of materials equipment and staff. The authors would also like to thank Zonguldak Karaelmas University, Institute of Science, and the Project and Science Research Commission for their support.

References

[1] Barnhouse EJ, Lippold JC. Microstructure/property relationship in dissimilar welds between duplex stainless steel and carbon steels. Welding J 1988;(December):477–87.
[2] Shaeffler AL. Constitution diagram for stainless steel weld metal. Metal Progr 1949:680B–1B.
[3] Delong WT. Ferrite in austenitic stainless steel weld metal. Welding J 53(7):273S–85S.
[4] Kotecki DJ, Siewert TA. Constitution diagram for stainless steel weld metals: a modification of the WRC-1988 diagram. Welding J 1992;5:171S–8S.
[5] Kotecki DJ. A martensite boundary on the WRC-1992 diagram – Part 2: The effect of manganese. Welding J 2000;(December):346S–54S.
[6] Rowe MD, Nelson TW, Lippold JC. Hydrogen-induced cracking along the fusion boundary of dissimilar metal welds. Welding J 1999;(February):31s–7s.
[7] Nelson TW, Lippold JC, Mills MJ. Nature and evolution of the fusion boundary in ferritic–austenitic dissimilar metal welds – Part 1: Nucleation and growth. Welding J 1999;(October):329–37.
[8] Nelson TW, Lippold JC, Mills MJ. Nature and evolution of the fusion boundary in ferritic–austenitic dissimilar metal welds – Part 2: On-cooling transformations. Welding J 2000;(October): 267–77.
[9] Tülbentçi K, Kaluç E. Paslanmaz Çelikler ve Kaynaklanabilirliği Seminer Notları''. Kocaeli Üniversitesi Kaynak Teknolojisi Araştırma Eğitim ve Uygulama Merkezi, Haziran, 1995, Kocaeli, Turkey.